

High quality amorphous silicon materials and cells grown with hydrogen dilution

Subhendu Guha, Jeffrey Yang, Arindam Banerjee, Baojie Yan and Kenneth Lord
United Solar Systems Corp.
1100 W. Maple Road
Troy, MI 48084

Key Words: amorphous silicon, solar cells, photovoltaics, microstructure, intermediate range order, hydrogen dilution

Abstract: Hydrogen dilution of the active gas during deposition has been found to be a very effective way to improve the quality of amorphous silicon based materials and solar cells. With increasing hydrogen dilution, the material is characterized by an improved order, and at a certain threshold dilution, the amorphous to microcrystalline transition takes place. The best material is grown just below the threshold, and is heterogeneous consisting of tiny crystallites embedded in an amorphous matrix of improved order. In this paper, we discuss the effects of hydrogen dilution on the material and cell properties of amorphous silicon based alloys, and provide explanation for their improved stability against light-induced degradation. We also discuss some special properties of the on-the-edge materials that are not seen in the conventional amorphous or microcrystalline alloys.

Email: sguha@uni-solar.com

Fax: 248.362.4442

Phone: 248.362.3120

1. Introduction

The low material cost and large-area deposition capability of amorphous silicon (a-Si) alloys have made this material a very viable candidate for commercial application of photovoltaics [1]. The lack of long-range order that increases the absorption coefficient of a-Si alloy also causes tailing of the bands that affect the transport of the carriers. Further deterioration of transport is caused by the presence of dangling and weak bonds, microvoids and other heterogeneities. Light-induced creation of metastable defects results in further degradation of performance, and a-Si alloy solar cells thus show poorer light-to-electricity conversion efficiency than their crystalline counterparts. While engineering innovations like the multi-junction approach [2] have led to substantial improvement of stable efficiency, there is a need to improve the intrinsic material quality of these alloys.

a-Si alloy is usually deposited by glow discharge decomposition of silane. It was first shown by Guha et al. [3] in 1981 that a-Si alloy films grown by decomposing a dilute mixture of silane in hydrogen show less light-induced degradation. The technique has been used successfully to make improved quality a-Si alloy [4], amorphous silicon-germanium (a-SiGe) alloy [5] and amorphous silicon-carbon alloy [6]. In fact it is now widely used by the entire photovoltaic industry to obtain high quality materials and devices, and has made the largest contribution to the improvement of stabilized cell and module efficiency. Simultaneously, much greater understanding has emerged in determining the role of hydrogen in improving material quality.

In this paper, we shall discuss the effect of hydrogen dilution on plasma chemistry and growth, structure and electronic quality of the material, and cell stability. We shall also review our current understanding as to why hydrogen dilution reduces light-induced degradation in solar cells.

2. Experimental

A typical glow discharge process consists of breaking up the active gas in a vacuum chamber by applying a suitable voltage through a pair of electrodes (Fig. 1). A radio-frequency source operating at 13.56 MHz is usually used, although very high frequency discharge has been used extensively to obtain higher deposition rates. In addition to hydrogen dilution, many other factors contribute to material quality. The best films are usually grown at chamber pressure between 0.1 to 1 torr, electrode distance between 4 to 6 cm, substrate temperature between 100 to 300 °C, and power density of 10 to 100 mW/cm². Typical hydrogen dilution range investigated is between 0 to 200. At a certain threshold of hydrogen dilution, a transition from amorphous to microcrystalline growth takes place. The best material is grown just below the threshold [7] and is characterized by improved intermediate range order. The exact dilution at which the transition takes place depends on the other deposition conditions and reactor design. It is customary to increase the dilution to observe experimentally where the transition occurs, and then reduce the dilution to work

slightly below the edge. This optimized material is often referred to as the 'edge' material.

3. Plasma Chemistry and Growth Kinetics

The basic plasma chemistry prevalent in a discharge of silane with or without hydrogen dilution has been investigated extensively [8,9]. Electron-molecule collisions dissociate the molecules into ions and neutral radicals. These radicals undergo various secondary reactions during their transport to the substrate. Of the various species (SiH, SiH₂, SiH₃, Si_xH_y etc.) in the plasma, SiH₃ has the longest life time. Bonding of SiH₃ to the growing surface needs dangling bonds, and removal of hydrogen from the surface is a necessary step in the deposition of films from SiH₃. Hydrogen can be released from the surface by thermal excitation, or it can be stripped by SiH₃ reacting with SiH to form a dangling bond and silane. Another SiH₃ molecule migrating along the surface or arriving directly can then be incorporated in the film leading to growth.

What is the role of excess hydrogen in the plasma? It provides improved surface coverage that results in the impinging molecules diffusing further to find more energetically favorable sites [10]. Hydrogen dilution should, therefore, result in a more ordered structure; in fact, with increasing hydrogen dilution, one should expect growth of microcrystallites. This has been known for a long time. Hydrogen is also an etchant. During the deposition process, both ordered and disordered regions may be

deposited simultaneously, and hydrogen etches away the disordered regions more effectively leaving behind the ordered structure [11]. An alternative explanation for obtaining a more ordered structure with hydrogen dilution is the phenomenon of chemical annealing [12]. This model postulates the structural relaxation of the amorphous phase and transition to crystalline phase by permeation of hydrogen atoms to a sub-surface region. It has been recently [13, 14] demonstrated that atomic hydrogen can be inserted into strained Si-Si bonds in the sub-surface region through the formation of a SiH_n complex. Subsequent structural relaxation of these bonds results in the growth of a more ordered phase. Molecular dynamics simulations also support this model [14].

While all the above models are consistent with the observation of improved order with increasing hydrogen dilution, an alternative explanation has been put forward [15] on the basis of formation of silicon powder (nano-clusters) in the plasma and their subsequent incorporation in the film. The deposition conditions and the hydrogen dilution are similar to those that have been used for obtaining high-quality materials described earlier. In most laboratories, however, one tries to avoid powder formation in the plasma since incorporation of powder can cause poor yield in devices.

4. Film Structure

The first systematic investigation of the effect of hydrogen dilution on the structure of a-Si alloys was carried out by Tsu et al [7] using high-resolution transmission electron microscopy (TEM) and Raman spectroscopy. The TEM results showed that embedded in the amorphous matrix are chain-like objects (CLO) having ~ 3 nm widths, ~ 30 nm lengths, and having a high degree of order along their length. Such order implies vanishingly small bond-angle distortion. The density of the CLO's increases with increasing hydrogen dilution. At very high hydrogen dilution, TEM results show the formation of microcrystallite inclusions; it is interesting to point out that small microcrystallites are observed even in films that are deposited below the threshold under conditions that are used for making the intrinsic alloys for the highest quality cells.

Raman measurements show a continuous shift of the TO peak 475 cm^{-1} to higher wave numbers with increasing hydrogen dilution. The results are interpreted by assigning a TO band existing at 490 cm^{-1} that exists in all the samples but increases in magnitude with increasing hydrogen dilution. This band is inferred to be the signature of the intermediate ordered CLO's. The Raman peak associated with microcrystallites at $\sim 515\text{ cm}^{-1}$ is observed in over the edge samples.

X-ray diffraction (XRD) measurements have also been used [16] to investigate the structure of these films. A narrowing of the width of the first x-ray scattering peak is

observed with increasing hydrogen dilution indicating improved intermediate range order. Even in samples that do not show any evidence of microcrystallinity, the width is narrower in hydrogen diluted samples than in typical amorphous materials with no hydrogen dilution. At dilutions above the threshold, microcrystallites appear with significant narrowing of the width of the peak (3^0 as opposed to more than 5^0).

A thickness dependence of the structure of the films was also demonstrated by these studies [16]. Films of different thicknesses grown under the same deposition conditions show improvement in intermediate range order as the thickness increases.

Similar dependence of degree of order on hydrogen dilution was reported by Koh et al [17] using real time spectroscopic ellipsometry. A thickness versus hydrogen dilution phase diagram was proposed, and the region of the phase diagram near the phase boundary but below the onset was termed the 'protocrystalline' regime. Real time spectroscopic ellipsometry is an important tool to study the evolution of film growth, and the work has elucidated valuable information about structure of films and its correlation with device performance [18].

5. Infra-red Studies and Hydrogen Effusion

Infra-red studies [19] show the hydrogen content in the films grown below threshold dilution to be similar (8 to 10%) independent of dilution. The films also show predominantly monohydride bonding. The peak frequency for the wag mode is,

however, found to change from around 635-640 cm^{-1} to $\sim 620 \text{ cm}^{-1}$ as the dilution is increased. Since the wag frequency of H bonded on to (100) or (111) surfaces of crystalline silicon is $\sim 620 \text{ cm}^{-1}$, it was argued that this shows presence of microcrystallites in the films even though they are grown below the edge. This supports the conclusions reached from TEM and Raman measurements.

Hydrogen evolution from the films also shows different behavior with increasing hydrogen dilution during growth. While films grown with a low hydrogen dilution show evolution of hydrogen around 500 $^{\circ}\text{C}$ (Fig. 2), the high dilution samples show a peak at a much lower temperature [20]. This indicates a structural difference in the materials grown with high and low hydrogen dilution. Small Angle X-ray Scattering (SAXS) also shows that films grown with high hydrogen dilution show a microstructure in the direction of film growth. This is not seen in conventional films grown with no dilution.

An interesting explanation for the observed low temperature hydrogen evolution in the edge material has been provided by Mahan et al [19]. The edge material is found to crystallize at a lower temperature than the conventional one; hydrogen evolution is thus conjectured to result from crystallization of the numerous small Si crystallites contained in the film that act as a catalyst. Even if the volume fraction is low, these crystallites can contain large amount of hydrogen on the surfaces accounting for the total hydrogen content in the film. There would be thus spatial inhomogeneity of hydrogen in the film with the amorphous region having very low hydrogen content.

Since it has been postulated [21] that lower hydrogen content can give better stability against light-induced degradation, the improved stability of the edge material could also be attributed to this.

6. Photoluminescence

Photoluminescence (PL) has been used [22] to explore the intermediate range order in materials at the onset of microcrystallinity. With increasing hydrogen dilution, a blueshift of the 1.4 eV PL peak energy takes place together with a decrease in the band width. This is attributed to improved order in the material. A careful comparison of device performance and PL shows that PL is a very useful tool to determine microcrystalline fraction in these mixed phase materials. Further discussion on the use of PL to study light-induced changes will follow.

7. Defect Density

Sub-bandgap absorption [20] of a-Si alloy was measured by constant photocurrent method (CPM), and showed very little effect of hydrogen dilution on defect density (Table 1). Both the initial and degraded defect densities were similar within experimental uncertainty. The cell performance on the other hand was much better with high dilution.

It has been argued [23] that since CPM measurement are carried out on films parallel to the surface where as the cell performance is measured in the perpendicular direction, a better correlation may be obtained if the defect density could be measured in an actual cell structure. This is especially important if the material is heterogeneous as is the case with hydrogen diluted alloys. Drive-level capacitance profiling (DLCP) is an interesting tool [24] since it can measure defect density in the actual cell configuration. Measurements using DLCP[25] show improvements in defect density as the hydrogen dilution is increased. What is most interesting is the fact that the defect density shows a spatial non-uniformity in the on the edge material, with the density decreasing in the growth direction. This demonstrates the improvement of order with thickness confirming the earlier SAXS measurements.

8. Cell Performance

Detailed results on the best cell and module performance have been presented elsewhere in this issue [26]. Hydrogen dilution has played a key role in obtaining the highest stabilized efficiency. Typical results for a-Si and a-SiGe alloy cells are shown in Table 2. Both a-Si and a-SiGe alloy cells deposited using high hydrogen dilution not only show higher initial performance, but also maintain superior performance in the light-soaked state.

We have carried out systematic experiments to find out optimum hydrogen dilution for the component cells for a triple-junction structure [28]. Figure 3 shows the

dependence of V_{oc} versus hydrogen dilution for a-Si alloy solar cells deposited on stainless steel with three different i layer thicknesses, 1250 Å, 2500 Å, and 5000 Å. R refers to the standard dilution that we use in our laboratory for obtaining the highest cell efficiency. *Please note that in other papers appearing in this volume, "R" refers to actual dilution (i.e., hydrogen to silane ratio).* For each thickness series studied, we note that there exists a critical threshold dilution beyond which V_{oc} begins to drop and also shows a large dispersion. This is due to the fact that the growth of microcrystallites for on-the-edge cells gives rise to a heterogeneous structure. This structure contains lower band gap microcrystallites embedded in a higher bandgap amorphous matrix, causing the lowering and spreading of V_{oc} . As the dilution is further increased to beyond the threshold, V_{oc} decreases dramatically, and eventually converges to a low value of ~0.45 V. It is also noted that for the 5000 Å series, the onset of microcrystallinity takes place at a lower dilution value, while the threshold for the 1250 Å series occurs at a higher dilution value. It is easy to conclude that microcrystallites are more readily obtained in thicker films.

Table 3 lists the J-V characteristic of a-Si alloy solar cells on stainless steel having an i layer thickness of ~2500 Å. The cells were made using four different hydrogen dilutions, corresponding to near-optimum, optimum, on-the-edge, and over-the-edge conditions. It is obvious that the optimum dilution that gives the best cell performance is lower than on-the-edge dilution, and the over-the-edge cell exhibits a low V_{oc} , indicating a substantial microcrystalline inclusion. In addition, the on-the-edge cell has a poorer fill factor than the over-the-edge cell, probably due to its

heterogeneous structure having microcrystallites mixed into the amorphous matrix. It is interesting to point out that hydrogen dilution between the optimum and over-the-edge cells differs by only a factor of 1.5, but it can result in such a dramatic difference in the cell performance. For the best quality material, it is therefore advisable to find the 'edge' condition first and then reduce the hydrogen dilution in order to reach a more desirable region.

Hydrogen dilution effect on a-SiGe alloy solar cells deposited on stainless steel has also been studied. The intrinsic layers are $\sim 2500 \text{ \AA}$ and the cells are made with no band gap profiling for ease of evaluation. The bandgap of the cells is $\sim 1.6 \text{ eV}$, suitable for use in the middle cell of a triple structure. The cell performance is measured under AM1.5 illumination with a $\lambda > 530 \text{ nm}$ cut-on filter. Table 4 lists the J-V characteristics of four a-SiGe alloy cells for the near-optimum, optimum, on-the-edge, and over-the-edge conditions. Again, the on-the-edge cell shows a lowering of V_{oc} and output power. The over-the-edge cell exhibits the worst performance.

We have also studied a-SiGe alloy solar cells with a flat band gap of $\sim 1.4 \text{ eV}$ and an i layer thickness of $\sim 1250 \text{ \AA}$. For this study, we deposit the cells on stainless steel and use AM1.5 with a $\lambda > 530 \text{ nm}$ filter for evaluation. Table 5 summarizes the J-V results for the cells with four hydrogen dilutions. A trend similar to the case of middle cells is observed here.

The dependence of V_{oc} and FF on hydrogen dilution for the top, middle, and bottom cells in Tables 3-5 is plotted in Figs. 4 and 5, respectively. We have normalized the hydrogen dilution with respect to the optimum condition for each component cell. It is readily observed from Fig. 4 that V_{oc} is indeed a sensitive tool for studying near threshold cell characteristics. As one increases the hydrogen dilution and enters into the amorphous and microcrystalline mixed-phase region, the V_{oc} value exhibits a significant reduction. This effect is most pronounced in the a-Si alloy cells; however, a-SiGe alloy cells also show similar transitional behavior. The sharp drop in V_{oc} is accompanied by a reduction in FF as can be seen in Fig. 5. For the over-the-edge a-Si alloy cell, the FF is higher than the on-the-edge cell, reflecting a better transport property for the carriers in the device. However, this effect is not observed in the a-SiGe alloy cells.

In Fig. 6, we plot the power output versus hydrogen dilution for the top, middle, and bottom component cells listed in Tables 3-5. It is obvious that in order to achieve high efficiencies, one must first identify the onset of microcrystallinity, and then go to a slightly lower dilution level for optimum conditions. It is also important to point out that the exact optimum hydrogen dilution depends critically on many other factors such as nature of substrate material, reactor geometry, deposition temperature, pressure, and gas flows.

Figure 7 shows the thickness dependence of the V_{oc} of a-Si alloy solar cells as a function of hydrogen dilution. For each experiment, several devices are measured

and data recorded. For low dilutions (0.5R to R), the V_{oc} is essentially independent of the intrinsic layer thickness for up to 5000 Å, indicating that the intrinsic layer is still amorphous. In these samples, the variation of V_{oc} on a given substrate is very small. As the dilution is increased to 1.2R and for a thickness of less than 3000 Å, the V_{oc} remains nearly constant. Beyond 3000 Å, however, some cells exhibit lower V_{oc} . For a thickness of 5000 Å, the dispersion in V_{oc} becomes large, and the lowest value of V_{oc} is lower than that of the 3000 Å cell. For the 1.4R samples, the value of V_{oc} becomes progressively lower and shows a spread even for a 1600 Å-thick device. In fact, the dispersion for the 5400 Å sample is as large as 200 mV. A higher dilution of 1.6R resulted in a further decrease in V_{oc} . In addition, as the cell thickness reaches 5000 Å, there is a substantial microcrystalline inclusion in the device, which is reflected by the smaller spread in V_{oc} and its low value. At the highest dilution (2R), V_{oc} drops to ~0.5 V even for the smallest thickness. A factor-of-two change in hydrogen dilution can result in a substantial change in V_{oc} , from 1 V to 0.5 V. When the material is 'on the edge', any small variation in deposition conditions can push the material over the edge. As pointed out earlier, for the best quality material, it is thus advisable to find the "edge" conditions and then reduce the hydrogen dilution somewhat to arrive at a more desirable region.

The thickness dependence of V_{oc} on a-SiGe alloy solar cells with ~40% Ge has also been studied and the results are plotted in Fig. 8. The following observations are made. First, due to the narrow bandgap of the a-SiGe alloy, V_{oc} takes on lower values. Second, for a dilution of 1.4R, V_{oc} remains rather constant and without much

dispersion for a thickness of up to $\sim 3000 \text{ \AA}$. This is in contrast to the case of a-Si alloy where 1.4R has already resulted in a spread in V_{oc} (see Fig. 7). Third, the amorphous-to-microcrystalline transition occurs at $>1500 \text{ \AA}$ for the 1.9R cell, which is characterized by a lowering and spread in V_{oc} . This is again in contrast with the a-Si alloy in that a dilution of 2R has already pushed a-Si alloys over the edge. We should also point out that the optimization of a-SiGe alloy solar cells is more complex than the a-Si alloy cells. Other deposition parameters can significantly influence the cell performance. While the dependence of V_{oc} on the thickness and dilution can serve as a guide to establish the threshold for a given set of deposition parameters, one must also optimize other conditions to assure good cell performance.

From Figs. 7 and 8 it is observed that for a cell thickness of $\sim 2000 \text{ \AA}$, the spread in V_{oc} occurs near 1.4R for a-Si alloys, and near 1.9R for a-SiGe alloys. The fact that the critical dilution for amorphous-to-microcrystalline transition increases with incorporation of Ge is not surprising. We have discussed earlier, it is well known [5] that one can obtain more ordered material if the adatom mobility of the impinging species on the growing surface is large. Hydrogen dilution is believed to passivate the growing surface so as to increase the adatom mobility, and this explains the improved order with increasing hydrogen dilution resulting eventually in the formation of microcrystallites. The predominant species for the growth of high quality a-SiGe alloys are SiH_3 and GeH_3 . Since GeH_3 is heavier than SiH_3 , a higher hydrogen dilution is necessary as the Ge-content increases to give the GeH_3 species enough mobility at the growing surface.

We have previously shown [28] that profiling of Ge-concentration as a function of thickness increases the built-in field within the cell and helps the hole transport. The highest cell efficiency was obtained when the Ge-concentration was changed continuously with the amount being maximum near the p-i interface. Since the optimum hydrogen dilution depends on the Ge-concentration, we have changed the hydrogen dilution during the growth of the intrinsic layer as a function of thickness with the dilution being the largest when the Ge-content is the highest. The results on two cells of the same thickness, with and without profiling of hydrogen dilution during growth, are shown in Table 6. The cells were deposited on stainless steel substrates with silver/zinc oxide back reflector. Measurements were made under global AM1.5 illumination with a $\lambda > 610$ nm cut-on filter to more appropriately evaluate the a-SiGe alloy solar cells. It is clearly seen that hydrogen dilution profiling improves the fill factor of the cell, indicating a better transport property of the minority carriers.

It is also interesting to point out that profiling of hydrogen dilution improves the quality of both a-Si and a-SiGe alloy solar cells, but the profiling directions are different. For a-Si alloy cells, since there is a tendency toward transition to microcrystallinity with increasing thickness, the dilution has to be reduced as the film thickness increases. For the a-SiGe alloy with the graded bandgap structure, on the other hand, since the Ge-concentration increases as a function of thickness, the hydrogen dilution has to increase as the thickness increases.

A significant light-induced enhancement in the open-circuit voltage (V_{oc}) of heterogeneous silicon solar cells in the amorphous-to-microcrystalline transition region has been reported recently [29]. As discussed earlier, the dispersion in V_{oc} is rather large in the transition region, and it is possible to obtain solar cells containing the amorphous, mixed and the microcrystalline phase on the same substrate in a given run. Light soaking on a single substrate thus gives information about light-induced changes in all the three phases.

Figure 9 shows the light-soaking effect on solar cells with initial V_{oc} values ranging from ~ 0.5 V to ~ 1.0 V, encompassing the amorphous, heterogeneous and amorphous silicon phases. Light soaking was carried out under one-sun intensity at 50 °C for 20 hours. The results show that for the cells with $V_{oc} < 0.55$ V or $V_{oc} > 1$ V, light soaking caused a small reduction in V_{oc} . For those heterogeneous cells with 0.55 V $< V_{oc} < 1$ V, the change in V_{oc} (ΔV_{oc}) became positive and peaked at a value midway between 0.55 V and 1 V. A ΔV_{oc} value as high as 140 mV was observed for the cell with an initial V_{oc} of ~ 0.8 V. Also, note the symmetrical behavior of the ΔV_{oc} with respect to the peak position. Light-induced variations in V_{oc} were substantially restored upon annealing at 150 °C for 2 hours, also shown in Fig. 9. The magnitude of ΔV_{oc} depends on the i layer thickness, the i layer deposition temperature, the initial V_{oc} , and the light soaking intensity. Under an intense light soaking, a ΔV_{oc} as large as 150 mV has been observed for a cell with an initial V_{oc} of 0.7 V. This is more than 20% change.

Next, we present experimental results on applying a bias to the cell during light soaking [30]. We first selected two pairs of cells, one amorphous and one heterogeneous, each pair having similar initial current-voltage (I-V) characteristics. We then applied a -5V bias to one cell from each pair and simultaneously subjected the four cells to one-sun light soaking at 50°C. The I-V characteristics were measured after 16 hours of exposure. Table 7 lists the V_{oc} and fill factor (FF) for the cells before and after light soaking. Degradation in FF is expressed in terms of the ratio of ΔFF to $FF_{ini.}$, where ΔFF is the difference in FF due to light soaking, and $FF_{ini.}$ is the initial FF before light soaking.

One notes that light soaking the amorphous cells (A_1 and A_2) causes only a small change in V_{oc} . The FF of the cell with no bias (A_1) degraded by about 5%. The FF of the cell with 5V reverse bias (A_2) improved by about 3%, which is attributed to the characteristic reverse bias annealing effect [31]. The light soaking effect on the heterogeneous cells (B_1 , B_2), however, is quite different from the amorphous cells. The V_{oc} of the no bias cell (B_1) increased by about 50 mV, while that of the -5V biased cell (B_2) increased by only 17 mV. The FF of B_1 decreased by ~13%, but by only ~5% for B_2 . One can clearly see that there is a significant difference in light-induced degradation with reverse bias.

It is well known [32] that light exposure creates new defects in the material resulting from recombination of photogenerated electrons and holes (Staebler-Wronski effect or SWE). Applying a reverse bias to the cell reduces or eliminates the opportunity for

the carriers to recombine, thus the observed smaller FF degradation for cell B₂ after light soaking. The fact that ΔV_{oc} is also smaller for B₂ strongly suggests that the source for ΔV_{oc} is also suppressed by the applied reverse bias. In other words, for cell B₁ that was light soaked without bias, the recombination event that causes the SWE and FF degradation must also have caused the enhancement of V_{oc} . Once the recombination channel is reduced by applying a reverse bias, both ΔFF and ΔV_{oc} are diminished.

Based on the result of the first experiment, it appears that the recombination event causes the V_{oc} enhancement for the heterogeneous cells. We also know that carrier injection can result in recombination in the solar cell. This leads to our next experiment. We again selected cells from the amorphous and mixed phases, and subjected them to a +1 V forward bias in the dark at 25 °C for 16 hours. We then measured the I-V characteristics again and compared them to their initial values; the V_{oc} and FF data are listed in Table 8. It is readily observed that forward bias resulted in a V_{oc} enhancement of 68 mV for the heterogeneous cell (D), while the amorphous cell (C) showed much smaller variations. The FF of both cells degraded due to recombination of the injected carriers.

The fact that V_{oc} increases substantially for the heterogeneous cell (D) in the dark reveals that the phenomenon does not rely on photons to initiate. It is the recombination event that triggers the enhancement of V_{oc} , which we believe to be associated with a structural change in the material. It should also be pointed out that

ΔV_{oc} is relatively small for the amorphous cell (C). The reason is the same as that given earlier for the light-induced effect. When the material is sufficiently amorphous, a small change in the microstructure does not significantly affect the carrier transport. Only when the material is sufficiently heterogeneous, with microcrystallites exceeding certain threshold volume fraction, does the microstructure change affect the carrier transport. This is reflected in the V_{oc} enhancement of heterogeneous cells after light soaking.

We have discussed earlier the use of PL to obtain information about intermediate range order in the material. The observed light-induced change in V_{oc} has also been investigated by PL. Fig. 10 shows the magnitude of PL intensity and PL peak position for cells with different V_{oc} . It is clear that higher PL intensity and peak-energy position is associated with a more amorphous structure. The results of *in-situ* light soaking on a cell with an initial V_{oc} of 0.86 V is shown in Fig. 11. With light-soaking the PL intensity increases and the peak position also shifts to a higher energy indicating a decrease in the ordered region with light exposure. This accounts for the observed increase in V_{oc} as well.

Although the above evidences suggest a light-induced reduction in the volume fraction of the more ordered regions in the mixed phase material, the process is not clearly understood. Light exposure has been shown to cause structural changes in a-Si alloys and the reduction in the volume fraction of the microcrystallites could result from this structural change. Moreover, recent studies [33] show this effect larger in materials

near-the-edge supporting the view that this edge material is more prone to structural changes. Kaiser et al. [34] found that a hydrogen-plasma treatment induces crystallization of a-Si alloys but reduces the volume fraction of microcrystallites in microcrystalline material. Grain boundaries can produce a significant effect in the hydrogen-induced conversion of crystallites to amorphous silicon. Based on data from nuclear magnetic resonance and infrared spectroscopy for mixed-phase materials, most hydrogen clusters in the grain boundaries [35]. It is reasonable to assume that hydrogen content in the more ordered region is less than in the grain boundary. During light-soaking, the strained bonds at the grain boundary are broken; hydrogen moves in and terminates some of the broken bonds. This effectively causes the shell layer of the grain to become more disordered reducing the volume fraction of the ordered regions.

We should point out that we have investigated the above light-induced structural changes using X-ray diffraction and Raman spectroscopy, but no detectable changes could be observed after light-soaking.

Hydrogen dilution plays an important role in the growth of microcrystalline solar cells also. The best cells are grown just above-the-edge [36]. It is thus interesting that the distinction between amorphous and microcrystalline materials have become less clear now, and cells made with a mixed phase material with nano-structures on either side of the edge show the best performance. Since the edge material is unstable (and can be pushed off the edge very easily), there have been controversies in the determination as to whether the material is below or above the edge. A case in question is the recent

observation [37] that highest quality p-type material is proto-crystalline (below-the-edge) and not microcrystalline (above-the-edge) as reported earlier [38]. Obviously, the mixed phase material has emerged as a new class of material, and will continue to get a great deal of attention.

9. Mechanism for Improved Stability

What causes the improved stability in hydrogen diluted material against light-induced degradation? Since hydrogen dilution improves order in the material, and SWE is observed in amorphous materials only, it is reasonable to assume that hydrogen dilution will reduce SWE. Presence of excess hydrogen during growth also etches away the weak bonds, a potential cause for SWE. The presence of microcrystallites in the mixed phase material has also been postulated to reduce SWE [39]. It has been suggested that recombination events take place at the embedded crystallites where bonds are stronger, and cannot be broken. We have also mentioned previously the postulation that outside the microcrystallites, the amorphous matrix contains very little hydrogen. If SWE is related to presence of hydrogen in the material, the above suggests that even if recombination events take place in the amorphous region, SWE will be small.

Yan et al. [40] have shown that the annealing of light-induced defects also is faster in the hydrogen-diluted alloys. Cells made with high hydrogen dilution show a low activation energy of defect annealing and a narrow distribution of defect energy. This

results in a faster annealing of the light-induced defects in the edge material than in the conventional a-Si alloy, and contributes to lower light-induced degradation. It is generally believed that both creation and annealing of these defects involve hydrogen motion. Measurements of diffusion coefficient of hydrogen in materials grown with different hydrogen dilution may help us to understand this mechanism better.

10. Conclusion

Ever since the first observation of improved stability against light exposure of a-Si alloys grown with hydrogen dilution, a variety of tools have been used to obtain a better understanding of the phenomenon. Hydrogen dilution has been demonstrated to result in materials with improved order, and beyond a certain threshold, the transition from amorphous to the microcrystalline phase takes place. A new class of mixed phase materials has emerged that, when incorporated in a cell structure, show the highest cell efficiency, both for the so-called amorphous and microcrystalline solar cells. These materials are grown on either side of the edge of amorphous to microcrystalline transition. The below-the-edge material is the most explored, and is characterized by improved intermediate range order and a heterogeneous structure.

Acknowledgement

References

1. S. R. Ovshinsky, Solar Energy Mat. Sol., Cells **32** (1994) 443.
2. S. Guha, J. Yang and A. Banerjee, Prog. in Photovoltaics, **8** (2000) 141.
3. S. Guha, K. L. Narasimhan and S. M. Pietruszko, J. Appl. Phys. **52** (1981) 859.
4. J. Yang, X. Xu and S. Guha, Mater. Res. Soc. Symp. Proc., **336** (1994) 687. Y. Lee, L. Jiao, H. Liu, Z. R. H. Collins and C. R. Wronski, Tech. Digest Int. Photovolt. Sci. Eng. Conf., PVSEC-9 (1996) 643. L. Yang and L. F. Chen, Mater. Res. Soc. Symp. Proc., **336** (1994) 669.
5. X. Xu J. Yang and S. Guha, J. Non-Cryst. Solids, **198-200** (1996) 60. G. Ganguly and A. Matsuda, J. Non-Cryst. Solids, **198-200** (1996) 559.
6. Y. Lu, S. Kim, M. Gunes, Y. Lee, C. R. Wronski and R.W. Collins, Mater. Res. Soc. Symp. Proc., **336** (1994) 595 .
7. D. V. Tsu, B. S. Chao, S. R. Ovshinsky, S. Guha and J. Yang, Appl. Phys. Lett, **71** (1997) 1317.
8. A. Gallagher, J. Appl. Phys., **63** (1988) 2406.
9. A. Matsuda, Conf. Record 25th IEEE Photovoltaic Specialists Conf., IEEE, New York, (1996) 1029.
10. A. Matsuda, J. Non-Cryst. Solids, **59-60** (1983) 767.
11. C. C. Tsai, G. B. Anderson, R. Thomson, and B Wacker, J. Non-Cryst. Solids, **114** (1989) 151.
12. N. Shibata, K. Fukuda, H. Ohtoshi, J. Hanna, S. Oda, and I Shimizu, Mat. Res. Soc Symp. Proc., **95** (1987) 225.

13. H. Fujiwara, Y. Toyoshima, M. Kondo and A. Matsuda, *Mat. Res. Soc. Symp. Proc.* **609** (2000) A.2.1.1.
14. S. Sriraman, S. Agarwal, E. S. Aydil and D. Maroudas, *Nature*, **418** (2002) 62.
15. P. roca i Cabarrocas, *J. Non-Cryst. Solids*, **266** (2000) 31.
16. D. L. Williamson, *Mat. Res. Soc. Symp. Proc.* **557** (1999) 251.
17. J. H. Koh, Y. Lee, H. Fujiwara, C. R. Wronski and R. W. Collins, *Appl. Phys. Lett.*, **73**, (1998) 1526.
18. A. S. Ferlauto, R. J. Koval, C. R. Wronski, and R. W. Collins, *Appl. Phys. Lett.*, **80** (2002) 2666.
19. A. H. Mahan, J. Yang, S. Guha, and D. L. Williamson, *Phys. Rev. B*, (2000) 1677.
20. X. Xu, J. Yang and S. Guha, *J. Non-Cryst. Solids*, **198-200** (1996) 96.
21. A. H. Mahan and M. Vanecek, in *Amorphous Silicon Materials and Solar Cells*, edited by B. L. Stafford *AIP Conf. Proc.* **234** (1991) 195.
22. G. Yue, D. Han, D. L. Williamson, J. Yang, K. Lord, and S. Guha, *Appl. Phys. Lett.* **77** (2000) 3185.
23. X. Xu, J. Yang and S. Guha, *Appl. Phys Lett.* **62** (1993) 1399.
24. C. E. Michelson, A. V. Gelatos, and J. D. Cohen, *Appl. Phys. Lett.* **47** (1985) 412.
25. S. Guha, J. Yang, D. L. Williamson, Y. Lubianiker, J. D. Cohen and A.H. Mahan, *Appl. Phys. Lett.* **74** (1999) 1860.
26. J. Yang, A. Banerjee and S. Guha (this volume).
27. J. Yang and S. Guha, *Mat. Res. Soc. Symp. Proc.* **557** (1999) 239.

28. S. Guha, J. Yang, A. Pawlikiewicz, T. Glatfelter, R. Ross and S. R. Ovshinsky, Appl. Phys. Lett. **54**, (1989) 2330.
29. K. Lord, B. Yan, J. Yang and S. Guha, Appl. Phys. Lett. **79** (2001) 3800.
30. J. Yang, K. Lord, B. Yan, A. Banerjee and S. Guha, Mat. Res. Soc. Symp. Proc. (2002), to be published.
31. D. L. Staebler, R. S. Crandall and R. Williams, IEEE PVSC 15 (1981) 249.
32. See, for example, H. Fritzsche in Mat. Res. Soc. Symp. Proc. **467** (1997) 19.
33. E. Stratakis, S. Spanakis, P. Tzanetakis, H. Fritzsche, S. Guha and J. Yang, Appl. phys. Lett. **80**, (2002) 1734.
34. I. Kaiser, N. H. Hickel, W. Fuhs, and W. Pilz, Phys. Rev. B **58**, (1998) R1718.
35. J. Baugh, D. Han, A. Kleinhammes, and Y. Wu, Mater. Res. Soc. Symp. Proc. **664**, (2001) A27.4.
36. O. Vetterl, R. Carius, L. Houben, O. Kluth, A. Lambertz, A. Muck, B. Rech and H. Wagner, Solar Energy Mat. Sol. Cells, **62** (2000) 97.
37. R. J. Koval, C. Chen, G.M. Ferreira, A. S. Fertanto, J. M. Pearce, P.I. Rorm, C. R. Wronski, and R. W. Collins, Appl. Phys. Lett. **81** (2002) 1258.
38. S. Guha, J. Yang, P. Nath and M. Hack, Appl. Phys. Lett., **49** (1986) 218.
39. T. Kamei, P. Stradins, and A. Matsuda, Appl. Phys. Lett. **74** (1999) 1707.
40. B. Yan, J. Yang, K. Lord, and S. Guha, Mat. Res. Soc. Symp. Proc. **664** (2001) A.25.2.

Table 1. Defect density in films and efficiency of cells at different hydrogen dilution					
Sample No.	Description	N_s , initial (CPM) (cm^{-3})	N_s , degraded (CPM) (cm^{-3})	Pmax (initial) mw/cm ²	Pmax (degraded) mw/cm ²
#1	a-Si:H, 300°C, low H ₂ dilution	2.9 e15	2.9 e16	7.5	5.8
#2	a-Si:H, 300°C, high H ₂ dilution	4.4 e15	3.0 e16	7.6	6.4
#3	a-Si:H, 175°C, low H ₂ dilution	7.9 e15	3.0 e16	7.0	4.0
#4	a-Si:H, 175°C, high H ₂ dilution	5.0 e15	2.5 e16	7.5	6.1

Table 2. Characteristics of a-Si:H and a-SiGe:H cells in both initial and degraded states.					
Description	State	J_{sc} (mA/cm ²)	V_{oc} (V)	FF	P_{max} (mW/cm ²)
300°C, low dilution	Initial	12.3	0.94	0.65	7.5
	Degraded	11.6	0.91	0.55	5.8
300°C, high dilution	Initial	11.6	0.96	0.68	7.6
	Degraded	11.2	0.94	0.61	6.4
175°C, low dilution	Initial	11.4	0.96	0.64	7.0
	Degraded	9.5	0.91	0.46	4.0
175°C, high dilution	Initial	10.9	1.00	0.69	7.5
	Degraded	10.5	0.97	0.60	6.1
a-SiGe, low dilution	Initial	17.6	0.72	0.55	7.1
	Degraded	14.9	0.64	0.41	3.9
a-SiGe, high dilution	Initial	18.0	0.74	0.59	8.0
	Degraded	16.3	0.69	0.45	5.1

Table 3. J-V characteristics of a-Si alloy top cells on ss with four different hydrogen dilutions measured under AM1.5 illumination.

Hydrogen Dilution	J_{sc} (mA/cm ²)	V_{oc} (V)	FF	P_{max} (mW/cm ²)
near-optimum	10.04	1.018	0.732	7.48
optimum	9.88	1.028	0.761	7.73
on-the-edge	9.82	0.624	0.426	2.61
over-the-edge	8.95	0.459	0.562	2.31

Table 4. J-V characteristics of a-SiGe alloy middle cells on ss with four different hydrogen dilutions measured under AM1.5 illumination with a $\lambda > 530$ nm filter.

Hydrogen Dilution	J_{sc} (mA/cm ²)	V_{oc} (V)	FF	P_{max} (mW/cm ²)
near-optimum	10.70	0.738	0.596	4.71
optimum	10.60	0.756	0.654	5.24
on-the-edge	10.67	0.617	0.607	4.00
over-the-edge	10.94	0.447	0.439	2.15

Table 5. J-V characteristics of a-SiGe alloy bottom cells on ss with four different hydrogen dilutions measured under AM1.5 illumination with a $\lambda > 530$ nm filter.

Hydrogen Dilution	J_{sc} (mA/cm ²)	V_{oc} (V)	FF	P_{max} (mW/cm ²)
near-optimum	10.81	0.656	0.555	3.94
optimum	10.78	0.654	0.639	4.51
on-the-edge	11.35	0.494	0.453	2.54
over-the-edge	11.64	0.356	0.427	1.77

TABLE 6. J-V characteristics for $\lambda > 610$ nm of graded bandgap a-SiGe alloy solar cells with and without hydrogen profiling.

Hydrogen Profiling	J_{sc} (mA/cm ²)	V_{oc} (V)	FF	P_{max} (mW/cm ²)
Yes	9.25	0.782	0.642	4.64
No	9.35	0.785	0.608	4.46

Table 7. V_{oc} and FF values for the amorphous (A_1 and A_2), heterogeneous (B_1 , B_2 , C_1 , and C_2), and low voltage (D_1 and D_2) cells before and after light soaking with and without a -5V bias.

Sample	State	V_{oc} (V)	ΔV_{oc} (mV)	FF	$\Delta FF/FF_{ini.}$ (%)
A_1	initial	1.027		0.648	
A_1	16 hr, one sun, no bias	1.016	-11	0.611	-5.7
A_2	initial	1.027		0.648	
A_2	16 hr, one sun, -5V bias	1.035	+8	0.667	+2.9
B_1	initial	0.839		0.581	
B_1	16 hr, one sun, no bias	0.889	+50	0.503	-13.4
B_2	initial	0.837		0.585	
B_2	16 hr, one sun, -5V bias	0.854	+17	0.554	-5.3
C_1	initial	0.696		0.509	
C_1	16 hr, one sun, no bias	0.749	+53	0.434	-14.7
C_2	initial	0.700		0.508	
C_2	16 hr, one sun, -5V bias	0.706	+6	0.486	-4.3
D_1	initial	0.515		0.411	
D_1	16 hr, one sun, no bias	0.522	+7	0.385	-6.3
D_2	initial	0.520		0.431	
D_2	16 hr, one sun, -5V bias	0.511	-9	0.437	+1.4

Table 8. V_{oc} and FF values for the amorphous (E), heterogeneous (F), and low-voltage (G) cells before and after +1V forward bias in the dark.

Sample	State	V_{oc} (V)	ΔV_{oc} (mV)	FF	$\Delta FF/FF_{ini.}$ (%)
E	initial	1.023		0.676	
E	degraded	1.011	-12	0.638	-5.6
F	initial	0.853		0.594	
F	degraded	0.921	+68	0.548	-7.7
G	initial	0.496		0.609	
G	degraded	0.501	+5	0.592	-2.8

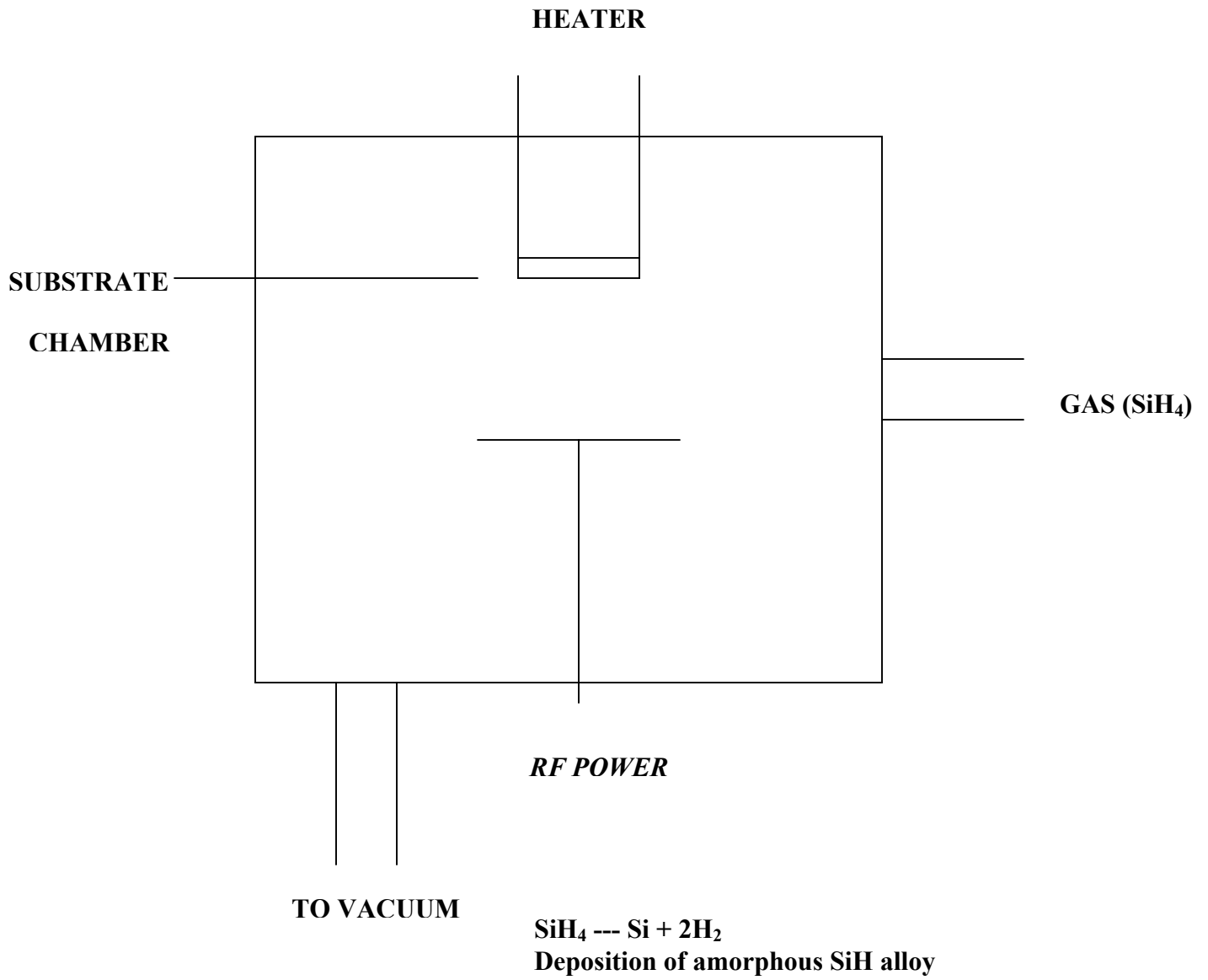


Fig. 1. Schematic diagram of a glow-discharge deposition reactor.

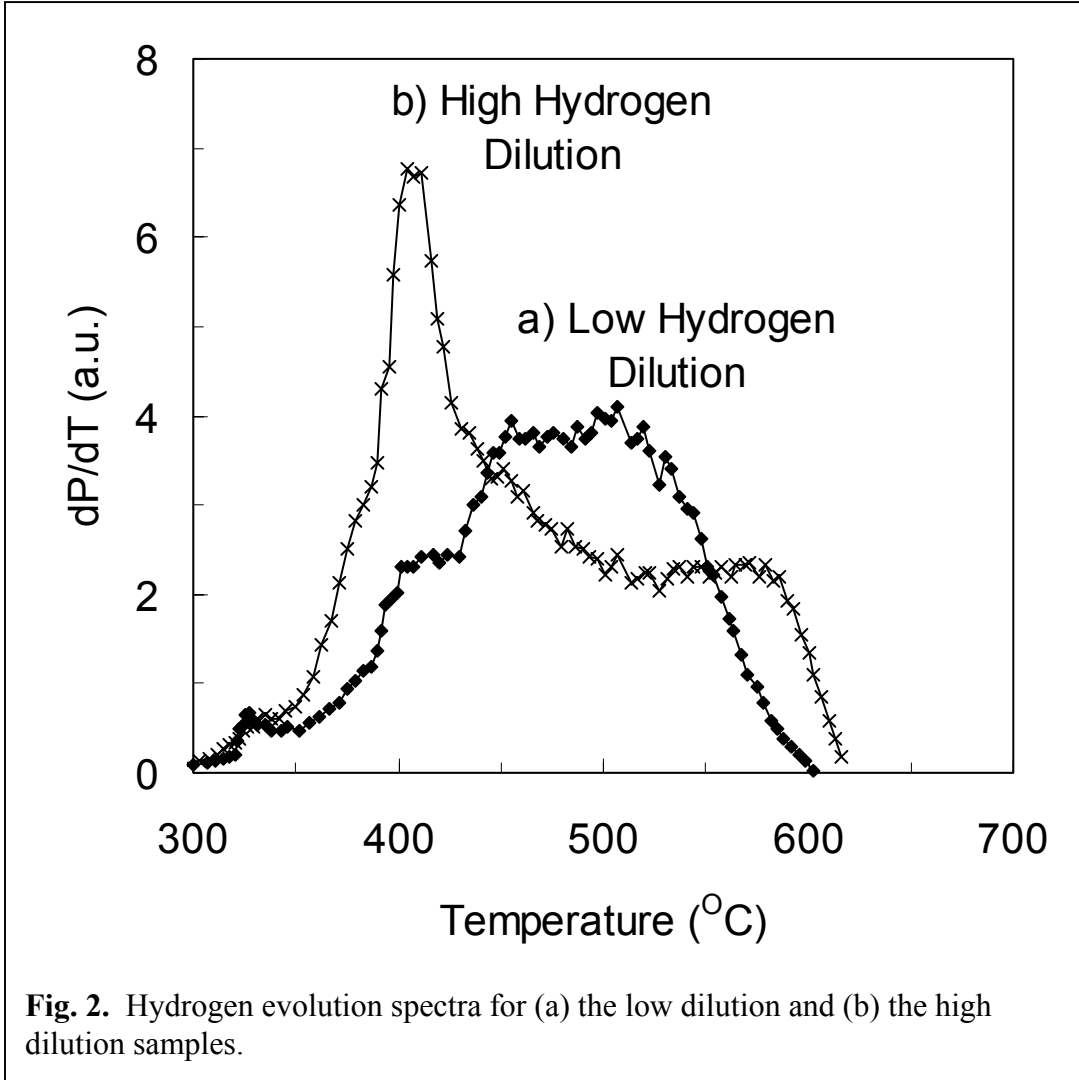


Fig. 2. Hydrogen evolution spectra for (a) the low dilution and (b) the high dilution samples.

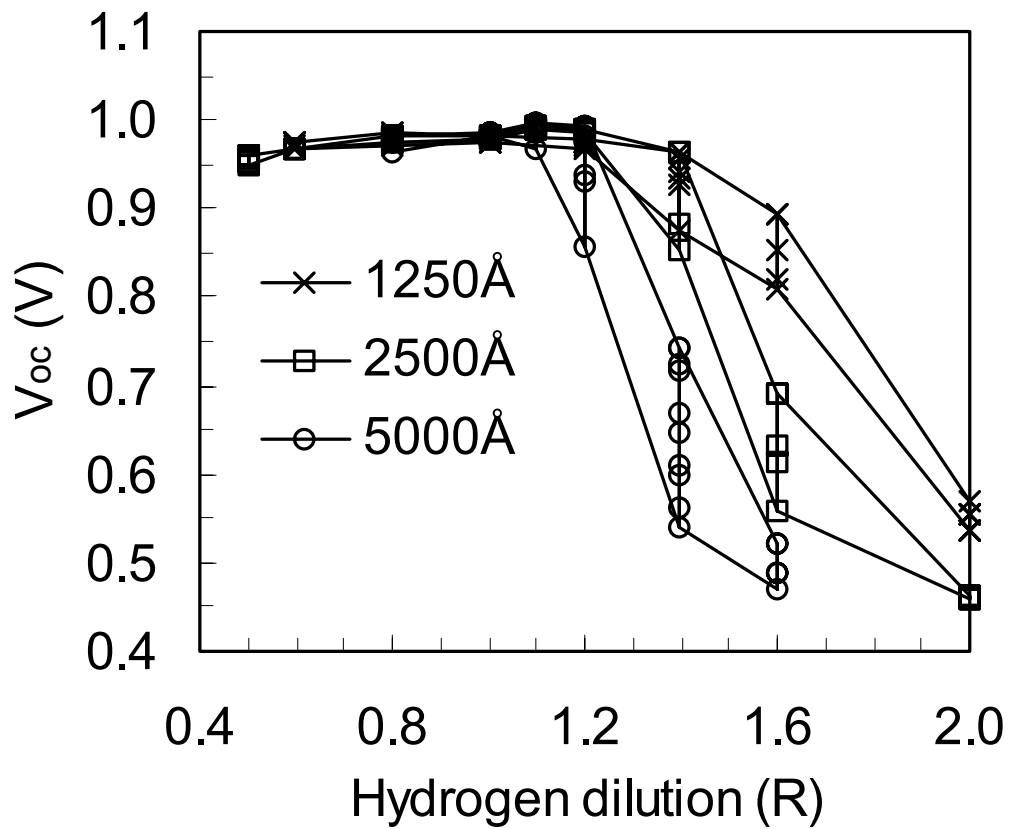


Fig. 3. Dependence of V_{oc} on hydrogen dilution for 1250 Å, 2500 Å and 5000 Å-thick a-Si alloy cells.

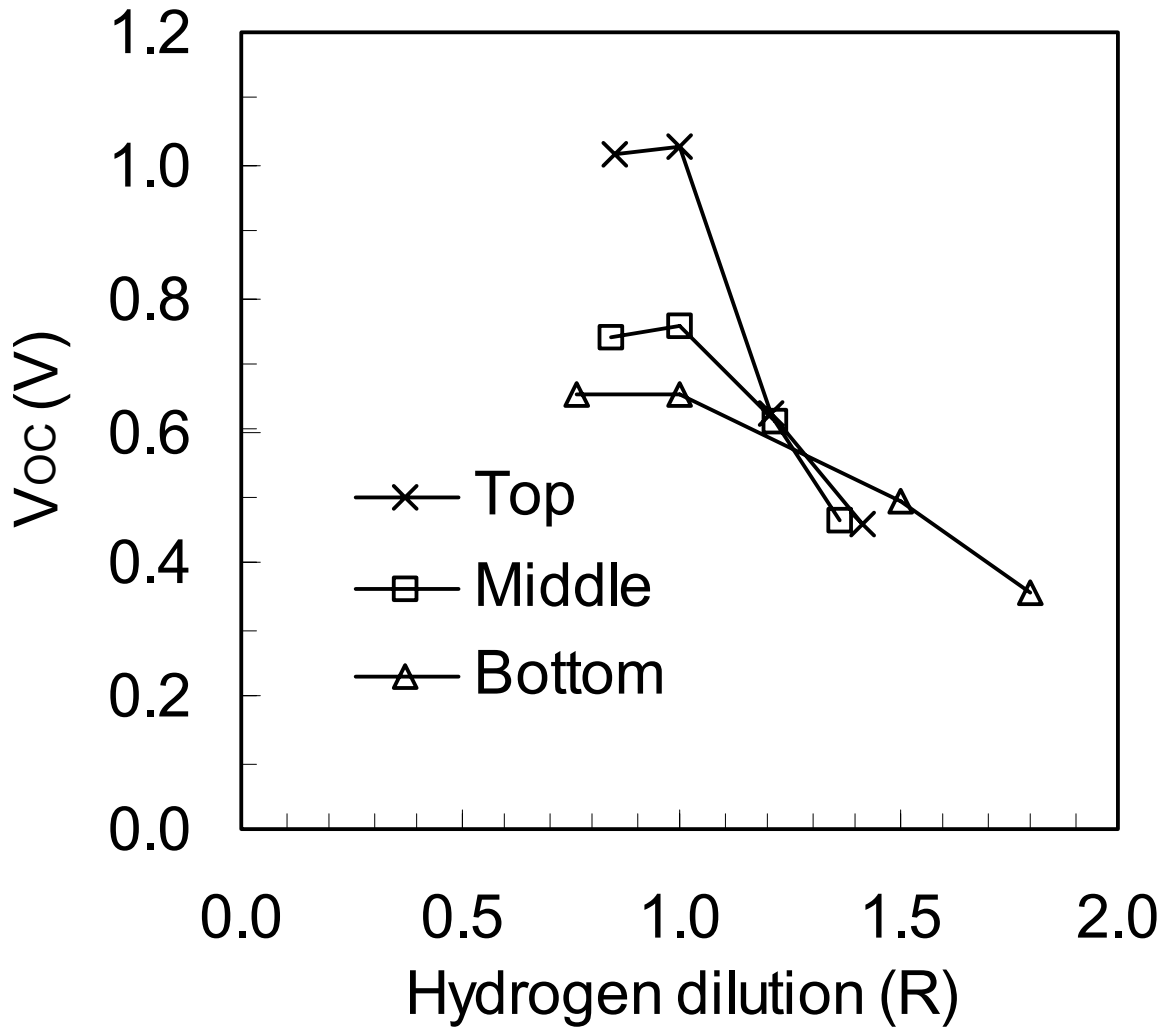


Fig. 4. Dependence of V_{oc} on hydrogen dilution for component cells.

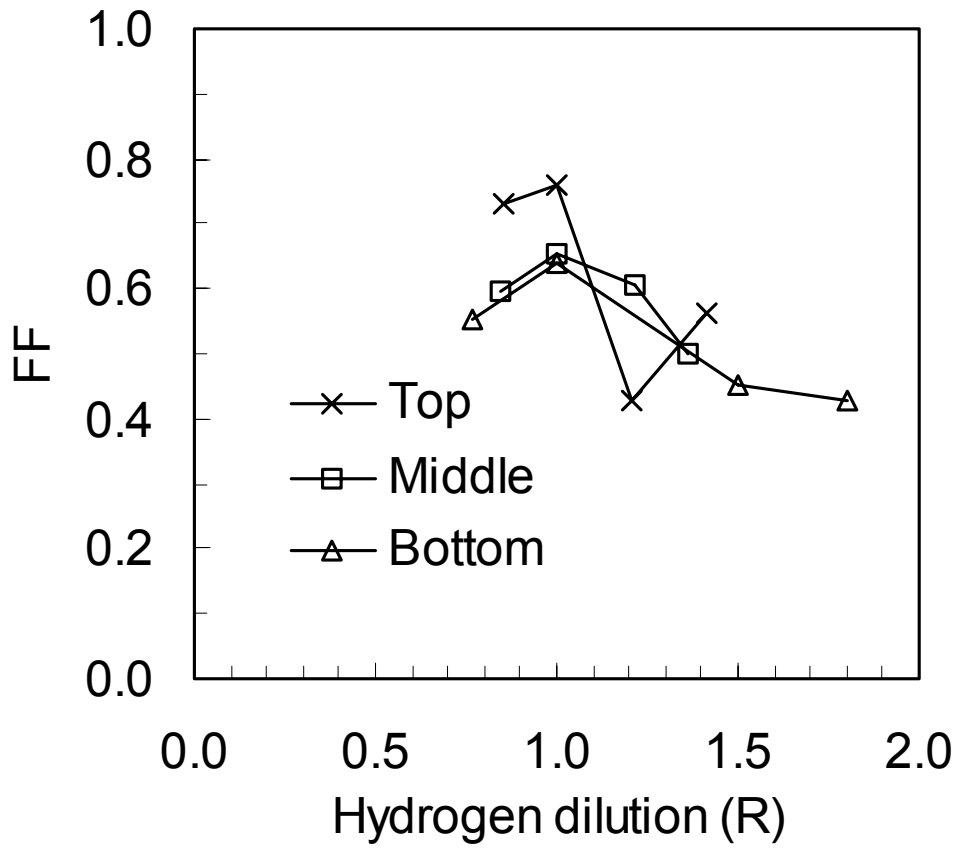


Fig. 5. Dependence of fill factor on hydrogen dilution for component cells.

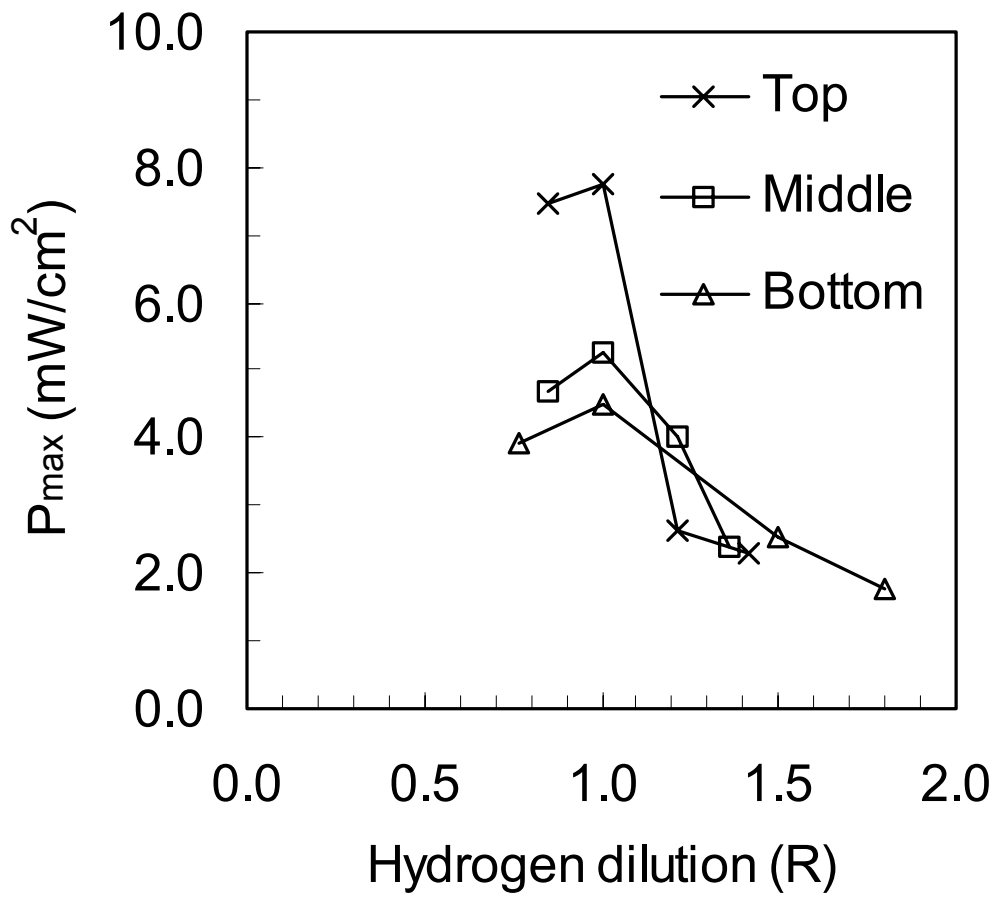


Fig. 6. Dependence of P_{\max} on hydrogen dilution for component cells.

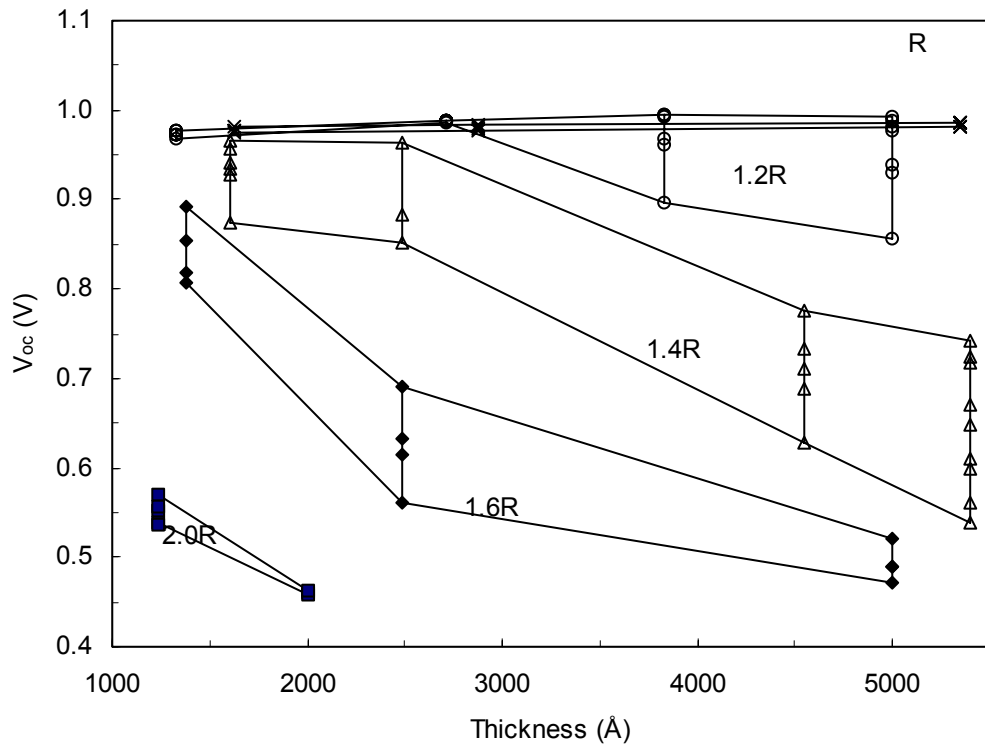


Fig. 7. Thickness dependence of V_{oc} of a-Si alloy cells deposited with different hydrogen dilutions.

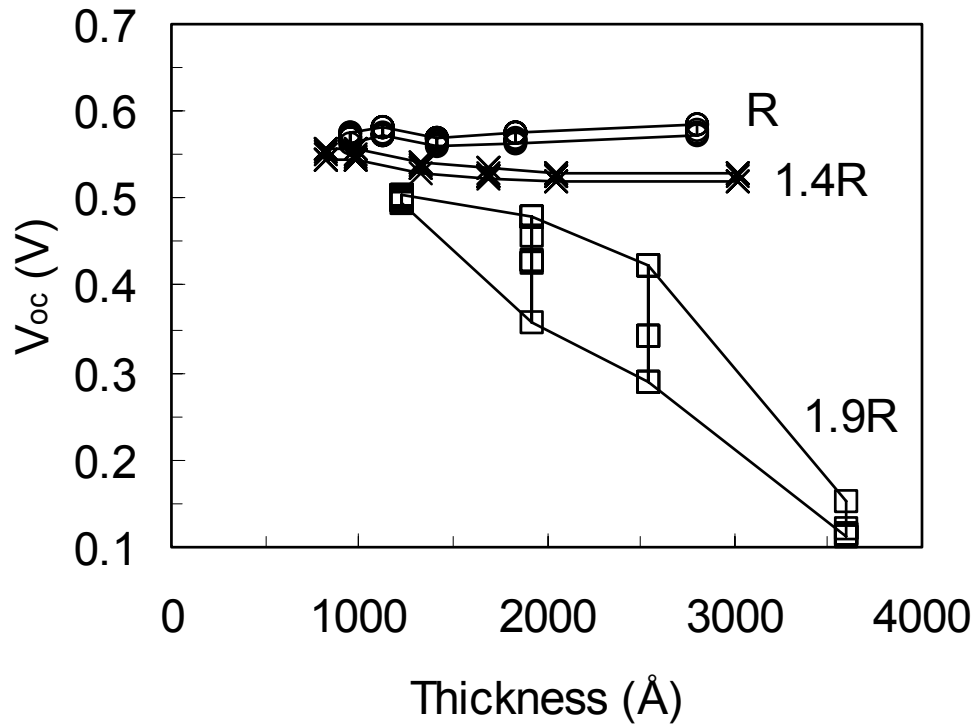


Fig 8. Thickness dependence of V_{oc} of a-SiGe alloy cells deposited with different hydrogen dilutions.

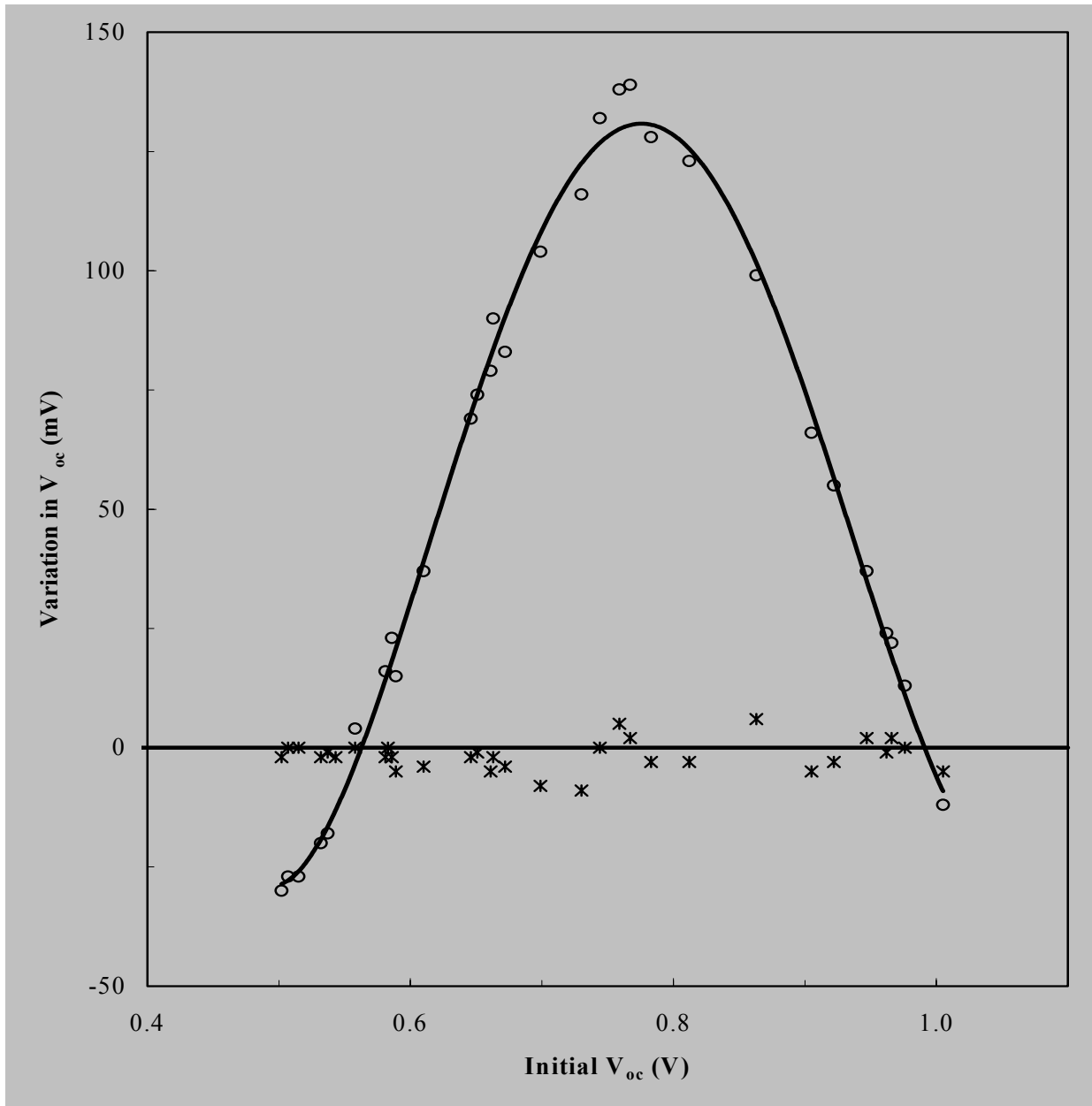


Fig. 9. ΔV_{oc} as a function of the initial V_{oc} for $\sim 5000 \text{ \AA}$ thick cells after one-sun light soaking for 20 hrs. (O). The line is a fit to the data and serves as a guide to the eye. Subsequent annealing at $150 \text{ }^\circ\text{C}$ for 2 hrs. (*) substantially restored the original V_{oc} values.

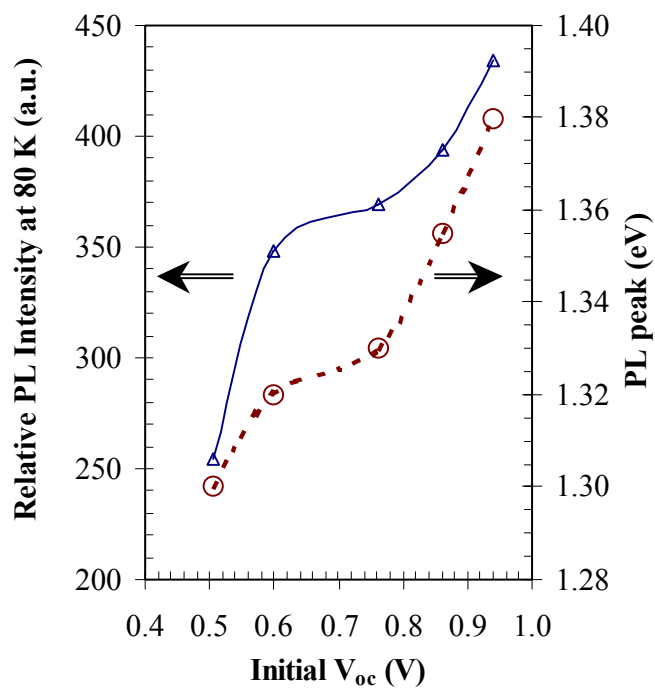


Figure 10. Relative PL intensity and peak energy position at 80 K as function of the initial V_{oc} .

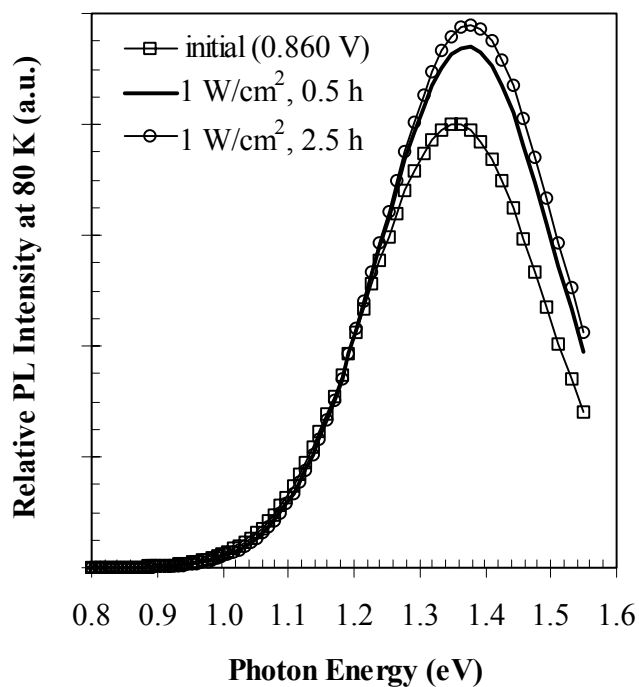


Figure 11. Effect of *in-situ* light soaking at room temperature by 1 W/cm² red light on the relative PL at 80 K.